14èmes Journées de l'Hydrodynamique

18-19-20 novembre 2014

DGA Techniques hydrodynamiques
Chaussée du Vexin
27105 Val de Reuil

A COMPARISON OF METHODS IN FULLY NONLINEAR BOUNDARY ELEMENT NUMERICAL WAVE TANK DEVELOPMENT

J.C. HARRIS*, E. DOMBRE*, M. BENOIT*, S.T. GRILLI**

* Laboratoire d'Hydraulique Saint-Venant, Université Paris-Est, Chatou, France
** Dept. of Ocean Engineering, University of Rhode Island, Narragansett, RI 02882, USA
jeffrey-externe.harris@edf.fr

Summary

We present the development and validation of an efficient numerical wave tank (NWT) solving fully nonlinear potential flow (FNPF) equations. This approach is based on a variation of the 3D-MII (mid-interval interpolation) boundary element method (BEM), with mixed Eulerian-Lagrangian (MEL) explicit time integration, of Grilli et al., which has been successful at modeling many phenomena, including landslide-generated tsunami, rogue waves, and the initiation of wave breaking over slopes. The MEL time integration is based on a second-order Taylor series expansion, requiring to compute high order time and space derivatives. In order to solve wave-structure interaction problems with complex geometries, we reformulate the model to use a 3D unstructured triangular mesh, building on earlier work, but presently only working with linear elements. The added flexibility of arbitrary meshes is demonstrated by modeling the longitudinal forces on a truncated (surface-piercing) vertical cylinder, comparing to theory and experiment. In order to improve the computational efficiency of the BEM, we apply the fast multipole method (FMM), in the context of the new unstructured mesh. A detailed study of the resulting computational time shows both the efficiency of the earlier 3D-MII approach and the proposed one, and also what is necessary to scale such results up to larger grids.

I – Introduction

Potential flow theory, which assumes irrotational (and thus inviscid) flows, has been very successful for modeling non-breaking water waves and wave-structure interactions, and is a standard tool in ocean engineering. Generally, at a given resolution, potential flow models have much less artificial dissipation than Navier-Stokes models, resulting in faster and more accurate results. Typically, in potential flow models, the boundary element method (BEM) is used to compute the solution for flows around ships and offshore structures. Numerous industrial wave models have been developed under this assumption, e.g., WAMIT [26], AQUAPLUS [5], and AEGIR [24]. Current numerical wave tanks (NWTs) based on the BEM have relatively similar approaches, as reviewed by Tanizawa [37]. The time-domain solution of fully nonlinear potential flow (FNPF) equations, however, requires solving an elliptic problem (Laplace's equation) with the BEM at each time step, which represents the biggest limitation of the method in terms of computational time,

even for moderately large grids; this is by contrast with standard linear frequency domain solutions (e.g., WAMIT) where only one BEM solution is performed per frequency. In the traditional BEM, for N degrees of freedom (DOFs), the assembly of a dense system of linear equations takes both a $O(N^2)$ computational effort and computer memory. Combined with a time step Δt that must be proportional to the grid resolution Δx (based on a constant mesh Courant number), BEM approaches for wave models have a CPU time that is $O[(\Delta x)^5]$, which is a severe limitation for fully nonlinear NWT development. It can often be sufficient to assume weak nonlinear effects, but this is not accurate for wave-structure interactions where large amplitude movements are expected, such as when modeling wave energy converters (WECs). The difficulty in obtaining both a fast (i.e., linearly scalable) and accurate BEM solution of Laplace's equation has led to new approaches [33], which for moderate-size problems may be promising, even if they do not achieve the same asymptotic $O(N)$ complexity as, e.g., the fast multipole method (FMM).

A typical solution to this scaling problem has been to develop NWTs based on higher-order elements, such as the cubic mid-interval interpolation (MII) elements [17, 14], for which fewer elements are required to achieve the same accuracy [29]; in this case, the complexity of a NWT comes from describing the geometry with the smallest number of DOFs possible. One such higher-order NWT was developed in three-dimensions (3D) by Grilli et al. [14], following earlier success in two-dimensions [16, 17] (2D), and has been used to model many wave phenomena, including landslide-generated tsunami [18], rogue waves [11], and the initiation of wave breaking over slopes [20]. Grilli et al.'s 2D-NWT was extended by Guerber et al. [19] to handle floating bodies, but the MII elements used in the NWT, while quite accurate, required a structured grid, which is difficult to apply to 3D surface-piercing bodies of complex geometry, such as ships, offshore structures, and WECs. Like most traditional BEM codes that are $O(N^2)$, Grilli et al.'s NWT becomes computationally inefficient for large grids, particularly in 3D. To overcome this limitation, Fochesato and Dias [10] implemented a FMM in the model (single CPU implementation), which theoretically provides a nearly $O(N)$ complexity, and Sung and Grilli [34, 35, 36] verified this performance beyond a few thousand DOFs for ship hydrodynamics problems. More recently, Nimmala et al. [31] extended the 3D-NWT with FMM to parallel computations, but due to complex details of the model algorithm the method could only be implemented on small shared memory clusters, whereas it is necessary to use distributed memory to best utilize large modern computer clusters. The FMM itself, however, pioneered by Greengard and Rokhlin [13], can be run on such large parallel computer architectures (see Yokota [38] for a recent review).

Here, we report on the implementation of the ExaFMM [39] in Grilli et al.'s 3D-NWT, using unstructured triangular grids to model interactions of waves with surface-piercing bodies. ExaFMM is one of the fastest FMM codes available today, which has been tested for billions of DOFs. Initial applications of this NWT have demonstrated its ability to predict nonlinear wave-induced forces on submerged bodies [27], and the favorable scaling of the FMM for large grids [21]. Here, we attempt to establish the NWT computational performance for wave interactions with surface-piercing bodies relative to existing, well validated approaches.

II – Methodology

In an incompressible fluid domain, D, if we assume inviscid and irrotational flow, then we can posit a velocity potential, ϕ, such that it satisfies Laplace's equation, and its

gradient is the fluid velocity, $\mathbf{u}$:

$$\nabla^2\phi = 0 \tag{1}$$

$$\mathbf{u} = \nabla\phi \tag{2}$$

at all times for all points in the domain. We also note that on the free surface :

$$\frac{D\phi}{Dt} = -gz + \frac{1}{2}\nabla\phi\cdot\nabla\phi + p_a \tag{3}$$

with the atmospheric pressure p_a assumed to be 0. These equations can be solved using a time stepping method with the MEL formalism of [30], in which Laplace's equation is expressed in an Eulerian coordinate system and the free surface and other moving parts of the boundary are then advected following fluid particle motions. The MEL can create multiple-valued free surface elevations, corresponding to overturning waves [20] ; here, to prevent this situation from occurring, which terminates simulations upon complete folding of the free surface, a semi-Lagrangian approach is used, in which free surface elevation is vertically adjusted, and fixed vertical boundaries are regridded at each time step to enforce evenly spaced elements and prevent poorly conditioned elements from occurring.

II – 1 Time integration

Here, following the developments of [14], in the tradition of Dold and Peregrine [6], we use an explicit 2nd-order Taylor series expansion to advance the free-surface variables (i.e., elevation and potential) in time. This requires first solving :

$$\nabla^2\phi = 0 \tag{4}$$

$$\frac{D\mathbf{x}}{Dt} = \mathbf{u} = \nabla\phi \tag{5}$$

$$\frac{D\phi}{Dt} = -gz + \frac{1}{2}\nabla\phi\cdot\nabla\phi \tag{6}$$

for the 1st-order terms, and then, using the same discretization, solving a second Laplace's equation for the 2nd-order terms :

$$\nabla^2\phi_t = 0 \tag{7}$$

$$\frac{D^2\mathbf{x}}{Dt^2} = \nabla\phi_t + \nabla(\frac{1}{2}\nabla\phi\cdot\nabla\phi) \tag{8}$$

$$\frac{D^2\phi}{Dt^2} = -gw + \mathbf{u}\cdot\frac{D\mathbf{u}}{Dt} \tag{9}$$

which, combined, yields :

$$\mathbf{x}(t+\Delta t) = \mathbf{x}(t) + \Delta t\frac{D\mathbf{x}}{Dt}(t) + \frac{(\Delta t)^2}{2}\frac{D^2\mathbf{x}}{Dt^2}(t) \tag{10}$$

$$\phi(t+\Delta t) = \phi(t) + \Delta t\frac{D\phi}{Dt}(t) + \frac{(\Delta t)^2}{2}\frac{D^2\phi}{Dt^2}(t) \tag{11}$$

This time stepping scheme has the advantage of making direct use of ϕ_t, which for many applications is also needed for computing hydrodynamic forces applied on the body surface anyway.

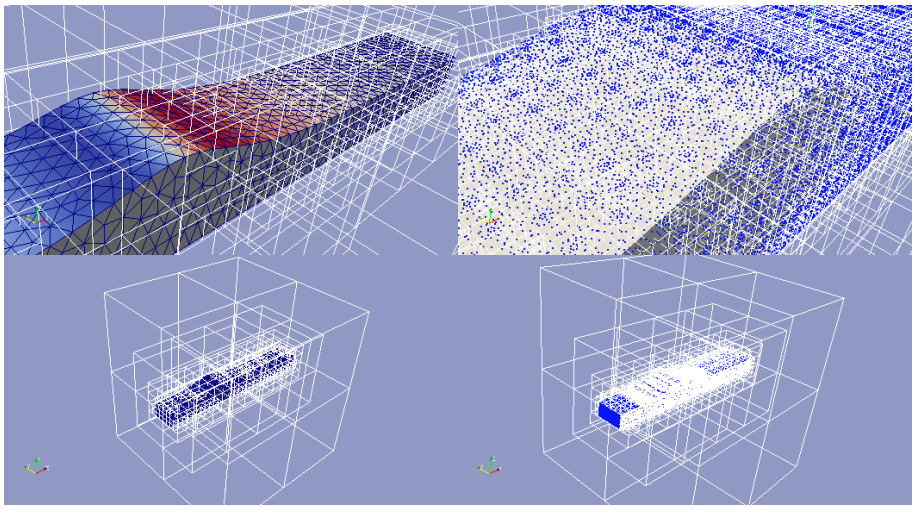

FIGURE 1 – Typical octree-structure of a NWT computational domain, in the case of solitary wave propagation. For neighboring cells, BEM integrals/interactions are computed using the free space Green's function ; for distant cells, integrals are computed through multipole expansions, saving computational effort.

II – 2 Solution of Laplace equation

We can rewrite Eq. 1 using Green's second identity as :

$$\alpha(\mathbf{x}_i)\phi(\mathbf{x}_i) = \int \left\{ \frac{\partial \phi}{\partial n}(\mathbf{x}) G(\mathbf{x}, \mathbf{x}_i) - \phi(\mathbf{x}) \frac{\partial G}{\partial n}(\mathbf{x}, \mathbf{x}_i) \right\} d\Gamma(\mathbf{x}) \tag{12}$$

where α is the solid angle at collocation point $\mathbf{x}_l$ on the domain boundary (e.g., 2π for a smooth boundary) and G the 3D free space Green's function of Laplace's equation :

$$G(\mathbf{x}, \mathbf{x}_i) = \frac{1}{4\pi |\mathbf{r}_i|} \tag{13}$$

$$\frac{\partial G}{\partial n}(\mathbf{x}, \mathbf{x}_i) = -\frac{1}{4\pi} \frac{\mathbf{r}_i \cdot \mathbf{n}}{|\mathbf{r}_i|^3} \tag{14}$$

where $\mathbf{r}_i = \mathbf{x} - \mathbf{x}_i$, is the distance to $\mathbf{x}$ also a point on the boundary, and n is the direction of the outward normal vector to the boundary.

In the collocation method, the Boundary Integral Equation (BIE), Eq. 12, is expressed for a series of points $\mathbf{x}_i$ defined as a grid over the domain boundary ; the latter being discretized in between those points by boundary elements, Γ_j. The BIE thus becomes a sum of integrals over each boundary element. For first-order triangular elements, regular integrations are performed using the Dunavant's [8] numerical quadrature rules, based on N_{intg} integration points ; singular integrals, which occur when integrating over the element containing a collocation node, are computed analytically. For additional details of the 3D-MII element model, see Grilli et al. [14]. We see from this BIE representation that, if we ignore singular integrals (which while critical for accuracy are not computationally time consuming), we are computing integrals representing "interactions" between pairs of collocation nodes (among N nodes), as a sum of values evaluated at N_{intg} integration points (Fig. 1). In the case of the 3D-MII model, each collocation node affects the velocity potential and flux on 16 adjacent elements, and generally $N_{intg} = 100$ integration points are used per element, so we expect $1600N^2$ evaluations of the BIE kernel are required to

assemble the algebraic system matrix. The iterative solution of this system also having a N^2 complexity, overall, we thus expect the complexity of the NWT solution for one time step to be $O(N^2)$.

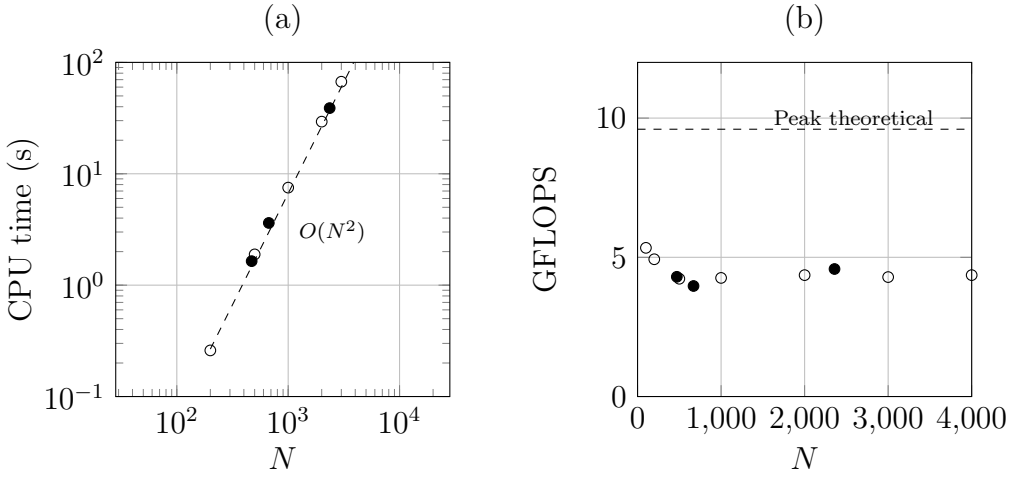

FIGURE 2 – Computational time of various n-body problems using 3D-MII code (•) and the equivalent direct (without FMM algorithm) computational effort with ExaFMM (○) : (a) CPU time for BIE system matrix assembling using Grilli et al.'s [14] NWT as a function of problem size N ; (b) Effective floating point operations, in GFLOPS, for the same problems – note that the maximum performance for one core of the hardware used here, an Intel Xeon E5620, is 9.6 GFLOPS.

While, particularly with modern computer architectures, we cannot expect to achieve the theoretical peak performance of a processor (see, e.g., Arora et al. [1] for explanations of some of the reasons), we can use the latter to see the computational efficiency of the 3D-MII code (Fig. 2). To do this, as in Grilli et al. [14], we propagate a solitary wave of large amplitude $H/h = 0.6$ over constant depth, and consider the average CPU time required for one time step versus the number of collocation nodes N, and we obtain the expected $O(N^2)$ complexity (in order to make the complexity more clear, adaptive integration, typically used near edges and corners in the NWT [14] was turned off). Assuming that 20 FLOPS are required for each evaluation of one interaction at one integration point, we can then compare the speed of the computation with the peak theoretical performance of the processor, and we see that we obtain about a 50% efficiency of the NWT for single core computations. In order to compare this with a dedicated n-body solver, to get a sense of whether this is a good result, we computed the interactions between $1600N$ source points and N target points, directly (not using the FMM capabilities), using the optimized ExaFMM library, and obtained effectively the same CPU time and efficiency (Fig. 2).

From this, we can see that the 3D-MII NWT is extremely efficient at assembling the system matrix, but also that if we wanted to significantly increase the size (N and hence NWT resolution for a given problem) of the NWT domain over what can be reasonably handled on a single core (i.e., a few thousand nodes), even if it were possible to perfectly distribute the computational load over multiple processors, the N^2 overall complexity of the solution would rapidly require using the largest computers possible.

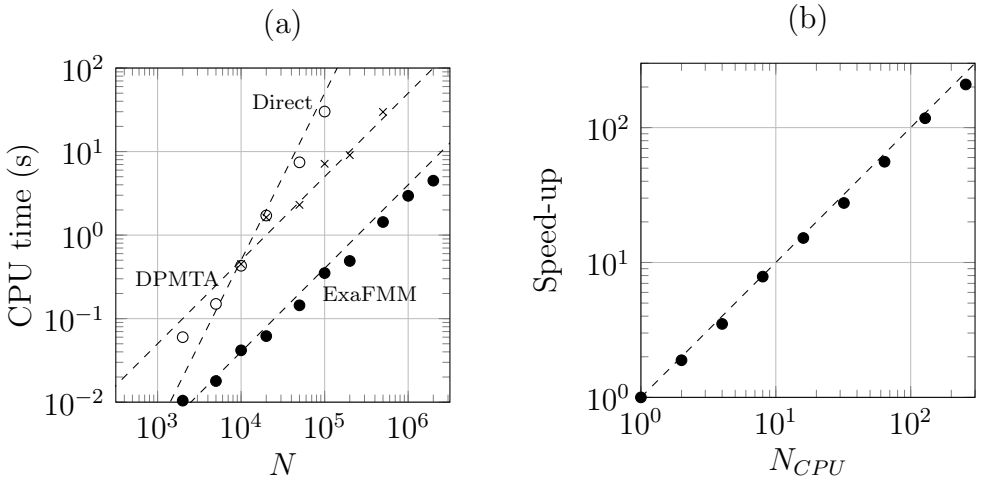

FIGURE 3 – Computational time of various n-body problems applied to the solitary wave domain (Fig. 1) : (a) CPU time for BIE system matrix assembling, using DPMTA, ExaFMM, and a direct computation using ExaFMM ; (b) CPU time scaling for fixed number of nodes $N = 10^6$, with increasing numbers of processors, using ExaFMM (calculations were done on a BlueGene/Q computer). Note that one processor of a BlueGene computer contains 16 computational cores, so this plot shows strong scaling to 4096 cores.

II – 3 Fast multipole method

The fast multipole method (FMM) is a tree-based algorithm (e.g., so-called octree in 3D ; Fig. 1) whereby, taking into consideration the $1/r_i$ behavior of the free space Green's function, the BIE interaction values between collocation points depends on the physical distance between them : interactions for nearby points are computed directly (using G) and those for distant points are computed through a multipole expansion (typically based on a Taylor's series or spherical harmonics, but there are many variations to the technique) ; in practice, beyond a cut-off distance depending on the number of terms in the expansion, interactions will be assumed to be negligible (i.e., zero). Hence, for large problems (N), the evaluation of all resulting interactions can be computed with a nearly $O(N)$ complexity. However, to solve the BEM with an iterative approach, even for a very sparse matrix, the number of iterations may increase with problem size, thus causing the overall complexity of the NWT solution to be higher ; using FMM, we previously found [21] $O(N^{1.3})$, which is consistent with other published FMM-BEM results.

As the use of the FMM introduces many complexities to the NWT, we first evaluated many existing FMM libraries, as there are many subtle differences between algorithms, which may affect overall computational speed. Yokota [38] performed such a comparison, testing many open source libraries on the same processor to get three digits of accuracy for the force of interacting particles randomly distributed in a cube. However, we have different requirements for accuracy and distribution of nodes, which may have an impact on performance (which was to some extent explored in earlier work [21]). This makes it necessary to reevaluate differences in speed using different FMM, when solving the same problem on the same computer in the NWT. Since Fochesato and Dias [10] had already implemented the FMM using the PMTA library [3] (v4.0, from 1994) in Grilli et al.'s [14] NWT, we will also test this library in the current NWT. Note, PMTA later evolved into DPMTA [32], which was used by Borgarino et al. [4] for other wave modeling problems

(using AQUAPLUS), but to our knowledge the library is no longer being developed. This will be compared with the ExaFMM, which we found in earlier work [21] to be the fastest among a group of other libraries.

Thus, in Fig. 2a, we see that ExaFMM is faster than DPTMA by nearly a factor of 10, while both libraries have the same $O(N)$ complexity, which contrast with the $O(N^2)$ complexity of the Direct method. We then solved the same problem with ExaFMM, using a fixed number of nodes $N = 10^6$ and an increasing number of processors/cores, up to 4,096 cores, on a BlueGene/Q system ; Fig. 2b shows that we obtain a nearly perfect linear scaling of CPU time speed-up. Each test case must be adapted to the computer architecture, however – for example, parallel performance on a BlueGene/Q machine is obtained using MPI, while on a single workstation, the multiple cores available are used by one of various threading tools, and MPI performance is not as good.

The next step in achieving such overall performance in the BEM-NWT is to relate the solution of Laplace's equation to the n-body problem, thus making it possible to benefit from the latest advancements in algorithms of the well established FMM field ; for instance, the 2012 Gordon-Bell prize winning paper was for a trillion particle n-body simulation [22], the largest such simulation achieved at the time. A collocation problem, as said, however, does not correspond precisely to a n-body problem, but $O(10^{12})$ integration points would correspond to $O(10^9)$ collocation nodes ; when then considering that $O(10^2)$ iterations are necessary to converge to a solution of Laplace's equation, we could consider that this method could, when fully developed, scale to $O(10^7 - 10^8)$ collocation points. That said, before using such massive computational resources, it is important to ensure that they are being used efficiently, which we consider in the next section.

II – 4 Computation of derivatives

The BEM collocation method solution provides both the velocity potential and its normal derivative on the computational domain boundary grid, at each time step. However, this is not sufficient to advance the solution in time using the 2nd-order Taylor series expansions. For this, we also need to compute higher-order tangential derivatives, which correspond to the tangential velocity and acceleration along the boundary, particularly the free surface and moving surface piercing bodies. So, the accurate computation of such derivatives is equally important to the solution as that of the BEM solution. For the 3D-MII technique, a 4th order polynomial fit to a sliding grid of 5x5 nodes was used, as detailed in Grilli et al. [14] and Fochesato et al. [12]. While the 3D-MII demonstrated exceptional accuracy for propagating a solitary wave and computing its overturning over a slope [20], to assess the new implementation of an unstructured mesh in the NWT for more realistic sea states, we should consider periodic waves with realistic tank dimensions and resolutions.

We first assess the solution's accuracy independently from time-stepping, by applying Dirichlet-Neumann boundary conditions for a test function Φ over a domain, solving for Φ_n on the free-surface, and considering the maximum relative error in the computed particle velocity. Thus, in Fig. 4, for various element models, we plotted the accuracy of the NWT solution for a box-shape domain (similar to Sung and Grilli [34, 36] or Shao and Faltinsen [33]), with dimensions $5\lambda \times \lambda \times \lambda/2$, for length, depth and width, respectively. when specifying an analytical wave-like potential on the free surface, $\Phi = \cos[(2\pi/\lambda)x] \exp[(2\pi/\lambda)z]$. We considered different discretizations N, and for each computed the accuracy in the velocity on the free surface.

We first see in Fig. 4a that, for the earlier 3D-MII cubic elements (with 4th-order

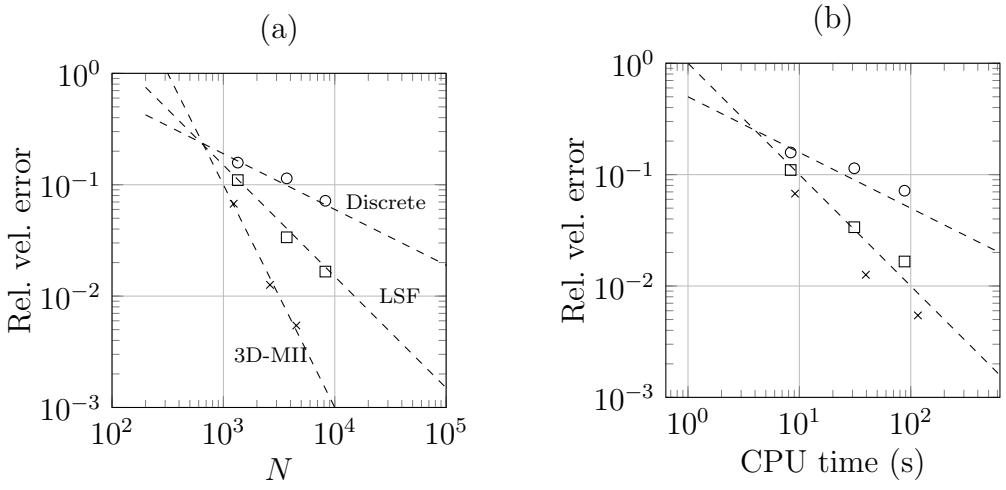

FIGURE 4 – Relative error in velocity on the free-surface, in the solution with Grilli et al. [14] NWT of an idealized Dirichlet-Neumann problem on a computational box, using an unstructured grid and an FMM-accelerated BEM, as a function of : (a) mesh size N : (b) CPU time. Only one time step is considered here and we compare the solution with standard 3D-MII cubic elements and 4th-order sliding derivatives, to that for an unstructured grid with linear triangular elements (Discrete and LSF method of derivatives).

sliding derivatives), we obtain the expected $O(N^2)$ convergence of the solution (as δx is proportional to N^2). Then, for an unstructured triangular grid, Fig. 5 shows the neighborhood of a collocation node. Considering element T_{ijk}, whose vertices are denoted by $\mathbf{x}_i$, $\mathbf{x}_j$, and $\mathbf{x}_k$, for linear shape functions, we can first express the velocity, i.e., the gradient of the potential, locally over T_{ijk}, as a sum of finite difference approximations over neighboring elements, weighted by the area of each element :

$$\nabla\phi_{T_{ijk}} = \frac{1}{2\mathcal{A}(T_{ijk})}((\phi_j - \phi_i)(\mathbf{x}_i - \mathbf{x}_k)^\perp + (\phi_k - \phi_i)(\mathbf{x}_j - \mathbf{x}_i)^\perp) \tag{15}$$

where $\mathcal{A}(T_{ijk})$ is the area of the triangular element T_{ijk}. Vector $(\mathbf{x}_i - \mathbf{x}_k)^\perp$ corresponds to the rotation of vector $\mathbf{x}_i - \mathbf{x}_k$ by an angle of $\frac{\pi}{2}$ in the direct sense. This is referred to as "Discrete" method in Fig. 4a, and we see a fairly poor convergence of errors, $O(N^{0.5})$ or so. Finally, we compute derivatives based on a least-squares fit (LSF). Given some values of the velocity potential and its normal derivative at nearby points, it is possible to fit a Taylor series expansion of this potential. The FMM already makes use of such a division for points in the neighboring volume and those that are far away, to compute such a series expansion. In order to enforce the condition that the resulting expression be harmonic, we use a 8th-order spherical harmonics fit to computed values at collocation nodes considered to be "local" in the FMM expansion. Fig. 4a shows a substantial improvement in accuracy, with a $O(N)$ convergence or so of the velocity, using the same linear element mesh as for the Discrete method.

A more interesting comparison than just error versus grid size is that of Fig. 4b, showing the CPU time of each model solution, for the grid and size required to achieve a given error in Fig. 4a. While the 3D-MII NWT converges much faster with N to the analytical solution, in terms of CPU time, however, the effort required to achieve a given error is quite similar to that of the unstructured linear triangular mesh with the LSF method. With higher-order boundary elements (e.g., splines), it might thus be possible to

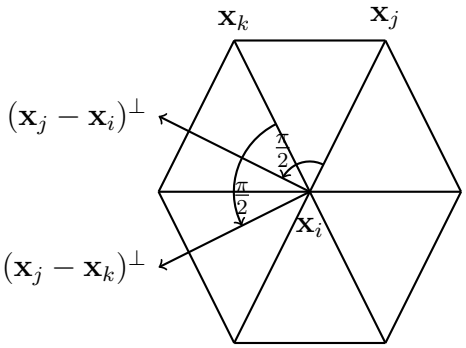

FIGURE 5 – Sketch of triangular element mesh T_{ijk}, also called the 1-ring neighborhood of the vertex $\mathbf{x}_i$.

surpass the 3D-MII performance on an unstructured grid.

III – Application to wave-structure interaction

Next, we compute wave interactions with a surface-piercing cylinder of radius R and draft D (Fig. 6), for the same problem setup as Liu et al. [28] ($D/R = 3$). They considered a truncated vertical cylinder in deep water, and compared their fully nonlinear BEM results to experimental results [25], frequency-domain computations [23], and small-body asymptotic theory of Faltinsen et al. [9]. Such a case is of particular interest because of the third-order ringing forces that can be important for offshore structures. We force the NWT with the kinematics of a theoretical periodic wave solution along a (leftward) wavemaker boundary. In order to reduce effects of reflection from the (rightward) end wall, similar to earlier work in two dimensions [15, 7], as in [2], we specify absorbing beaches (AB) by adding a dissipative term into the free surface boundary conditions, over an arbitrary length denoted by l_{AB}. For the dynamic boundary condition, this term here reads :

$$\frac{D\phi}{Dt} = -gz + \frac{1}{2}\nabla\phi \cdot \nabla\phi - \nu(\mathbf{x})\phi \tag{16}$$

(a) (b)

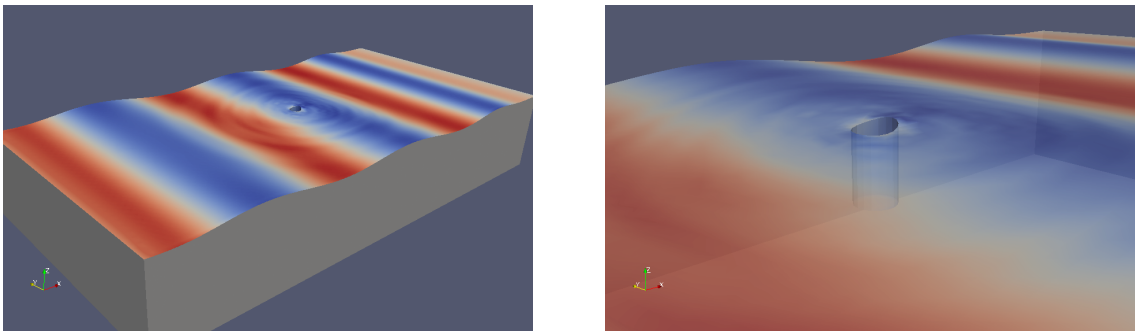

FIGURE 6 – Snapshot of free-surface vertical acceleration, showing incoming and diffracted waves around a surface piercing cylinder of radius R and draft D ($D/R = 3$ and $kR = 0.22$, for $k = 2\pi/L$; wavelength L) : (a) full-domain ; (b) close-up.

In addition, an equivalent term is introduced into the kinematic boundary condition which, for a semi-Lagrangian scheme, is expressed as :

$$\frac{Dz}{Dt} = w - \nu(\mathbf{x})z \tag{17}$$

with the vertical particle velocity $w = \phi_z$ and the damping term $\nu(\mathbf{x})$ being defined in terms of the coordinates x in the longitudinal direction as (for $x \geq x_{AB}$) :

$$\nu(\mathbf{x}) = \omega \left(\frac{x - x_{AB}}{l_{AB}} \right)^2 \tag{18}$$

and otherwise $\nu = 0$. In a similar fashion, we also control the free surface profile in front of the wavemaker by substituting in the previous equations, ϕ for $\phi - \phi_e$, and $z - z_e$, ϕ_e and z_e corresponding to an Airy wave (this reference solution could easily be replaced by a nonlinear wave theory, but for the case presented here the incoming wave is of small amplitude).

Result	Method	$\lvert f^{(1)}\rvert/(\rho g R^3)$	$\lvert f^{(2)}\rvert/(\rho g R^3)$
Experiments	Krokstad and Stansberg [25]	13.64	10.85
Second order BEM	Liu et al. [28]	13.41	12.97
Second-order freq. domain	Kim and Yue [23]	13.28	14.86
Small-body asympt. theory	Faltinsen et al. [9]	13.93	16.64
Present NWT	BEM (1st order elem.)	13.406	7.397

TABLE 1 – First and second order forces computed for a truncated vertical cylinder with $D/R = 3$, and $kR = 0.22$.

We consider a grid of $N = 8591$ collocation nodes (17194 elements), with 18 points around the waterline of the cylinder, and simulate 8 wave periods. The first-order force coefficient is easily computed (Fig. 7), which we see gives results identical to Liu et al. and is within the range of other results listed in Table 1. The agreement with the second-order force is less good, but there is considerable variation in earlier published results .

IV – Summary

We showed results of a new implementation of a FMM-accelerated BEM-NWT for wave-structure interactions, giving solution times competitive with existing methods. This approach solves in the time-domain for fully nonlinear potential flow, on unstructured 3D grids with linear triangular elements. If we compare the performance of this NWT with that of Grilli et al. [14], as expected, we see that the earlier NWT, which is higher-order, achieves better conservation of energy and volume, but it does not scale well in CPU time/numerical complexity, beyond a few thousand DOFs. By contrast the present NWT has the potential for achieving similarly accurate results with $O(N)$ scaling.

Further modifications of the present unstructured grid code are necessary to use higher-order elements. Still, we clearly see that the FMM is very efficient for solving Laplace's equation, and it is possible to use it with limited modification the established library ExaFMM [39]. Additional results, with finer grid resolution, and demonstrating the parallel performance of the complete NWT, will be shown at the conference.

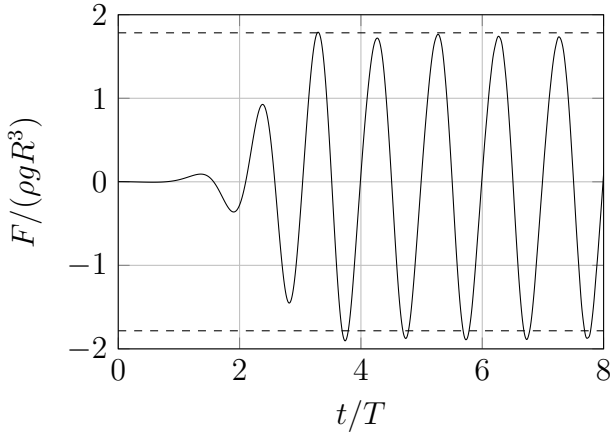

FIGURE 7 – Longitudinal force measured on a truncated cylinder in waves (same case as Fig.6), with the dotted line showing the magnitude predicted by Liu et al. [28], showing the rapid convergence to a periodic solution.

V – Acknowledgements

The work of J. Harris and M. Benoit is funded as a part of the French ANR (Agence Nationale de la Recherche), project ANR11-MONU-018-01 MONACOREV, and the work of E. Dombre by the ANRT (Association Nationale de la Recherche et de la Technologie), CIFRE agreement #2011-1724. S.T. Grilli acknowledges support from Grant N000141310687 of the US Office of Naval Research. We would like to thank Dr. Rio Yokota for useful discussions of the fast multipole method.

References

[1] N. Arora, A. Shringarpure, and R. W. Vuduc. Direct N-body kernels for multicore platforms. In *42nd Intl. Conf. on Parallel Processing*, pages 379–387, Vienna, Austria, 2009.

[2] W. Bai and R. Eatock Taylor. Higher-order boundary element simulation of fully nonlinear wave radiation by oscillating vertical cylinders. *Applied Ocean Research*, 28 :247–265, 2006.

[3] J. A. Board, Z. S. Hakura, W. D. Elliott, and W. T. Rankin. Scalable variants of multipole-based algorithms for molecular dynamics applications. Technical Report 94-006, Duke University, Department of Electrical Engineering, 1995.

[4] B. Borgarino, A. Babarit, and P. Ferrant. Extension of the free-surface green's function multipole expansion for the infinite water depth case. In *Proceedings of the 20th International Offshore and Polar Engineering Conference*, pages 802–809, 2010.

[5] G. Delhommeau. Seakeeping codes AQUADYN and AQUAPLUS. In *Offshore Structures : 19th WEGEMT School*, 1993.

[6] J. W. Dold and D. H. Peregrine. Steep unsteady water waves : an efficient computational scheme. In *Proceedings of the International Conference of Coastal Engineering*, pages 955–967, Houston, TX, USA, 1984.

[7] E. Dombre, M. Benoit, D. Violeau, C. Peyrard, and S. T. Grilli. Simulation of floating structure dynamics in waves by implicit coupling of a fully nonlinear potential flow model and a rigid body motion approach. *J. Ocean Engng. and Marine Energy*, (accepted).

[8] D. A. Dunavant. High degree efficient symmetrical Gaussian quadrature rules for the triangle. *International Journal for Numerical Methods in Engineering*, 21 :1129–1148, 1984.

[9] O. M. Faltinsen, J. N. Newman, and T. Vinje. Nonlinear wave loads on a slender vertical cylinder. *Journal of Fluid Dynamics*, 289 :179–198, 1995.

[10] C. Fochesato and F. Dias. A fast method for nonlinear three-dimensional free-surface waves. *Proceedings of the Royal Society A*, 462 :2715–2735, 2006.

[11] C. Fochesato, S. T. Grilli, and F. Dias. Numerical modeling of extreme rogue waves generated by directional energy focusing. *Wave Motion*, 44 :395–416, 2007.

[12] C. Fochesato, S. T. Grilli, and P. Guyenne. Note on non-orthogonality of local curvilinear co-ordinates in a three-dimensional boundary element method. *International Journal for Numerical Methods in Fluids*, 48 :305–324, 2005.

[13] L. Greengard and V. Rokhlin. A fast algorithm for particle simulations. *Journal of Computational Physics*, 73 :325–348, 1987.

[14] S. T. Grilli, P. Guyenne, and F. Dias. A fully nonlinear model for three-dimensional overturning waves over arbitrary bottom. *International Journal for Numerical Methods in Fluids*, 35 :829–867, 2001.

[15] S. T. Grilli and J. Horrillo. Generation and absorption of fully nonlinear periodic waves. *Journal of Engineering Mechanics*, 123 :1060–1069, 1997.

[16] S. T. Grilli, J. Skourup, and I. A. Svendsen. An efficient boundary element method for nonlinear water waves. *Engineering Analysis with Boundary Elements*, 6 :97–107, 1989.

[17] S. T. Grilli and R. Subramanya. Numerical modeling of wave breaking induced by fixed or moving boundaries. computational mechanics. *Computat. Mech.*, 17(6) :374–391, 1996.

[18] S. T. Grilli, S. Vogelmann, and P. Watts. Development of a 3d numerical wave tank for modeling tsunami generation by underwater landslides. *Engineering Analysis with Boundary Elements*, 26(4) :301–313, 2002.

[19] E. Guerber, M. Benoit, S. T. Grilli, and C. Buvat. A fully nonlinear implicit model for wave interactions with submerged structures in forced of free motion. *Engineering Analysis with Boundary Elements*, 36 :1151–1163, 2012.

[20] P. Guyenne and S. T. Grilli. Numerical study of three-dimensional overturning waves in shallow water. *Journal of Fluid Mechanics*, 547 :361–388, 2006.

[21] J. C. Harris, E. Dombre, M. Benoit, and S. T. Grilli. Fast integral equation methods for fully nonlinear water wave modeling. In *Proceedings of the 24th International Offshore and Polar Engineering Conference*, pages 583–590, Busan, Korea, 2014.

[22] T. Ishiyama, K. Nitadori, and J. Makino. 4.45 Pflops astrophysical N-body simulation on K computer - the gravitational trillion-body problem. In *Proceedings of the International Conference on High Performance Computing, Networking, Storage and Analysis*, page 10 pp., Salt Lake City, UT, USA, 2012.

[23] H. M. Kim and D. K. P. Yue. The complete second-order diffraction solution for an axisymmetric body. Part I. Monochromatic incident waves. *Journal of Fluid Dynamics*, 200 :235–264, 1989.

[24] D. C. Kring, F. T. Korsmeyer, J. Singer, D. Danmeier, and J. White. Accelerated nonlinear wave simulations for large structures. In *7th International Conference on Numerical Ship Hydrodynamics*, Nantes, France, 1999.

[25] J. R. Krokstad and C. T. Stansberg. Ringing load models verified against experiments. In *Proceedings of the International Conference on Offshore Mechanics and Arctic Engineering*, Copenhagen, Denmark, 1995.

[26] C. H. Lee. WAMIT Theory Manual. Technical report, MIT, 1995. Report 95-2, Department of Ocean Engineering.

[27] L. Letournel, J. C. Harris, P. Ferrant, A. Babarit, G. Ducrozet, E. Dombre, and M. Benoit. Comparison of fully nonlinear and weakly nonlinear potential flow solvers for the study of wave energy converters undergoing large amplitude motions. In *Proceedings of the 33rd International Conference on Ocean, Offshore and Arctic Engineering*, page 23912, San Francisco, USA, 2014.

[28] Y. Liu, M. Xue, and D. K. P. Yue. Computations of fully nonlinear three-dimensional wave-wave and wave-body interactions. Part 2. Nonlinear waves and forces on a body. *Journal of Fluid Dynamics*, 438 :41–66, 2001.

[29] Y. H. Liu, C. H. Kim, and X. S. Kim. Comparison of higher-order boundary element and constant panel methods for hydrodynamic loadings. *International Journal of Offshore and Polar Engineering*, 1 :8–17, 1991.

[30] M. S. Longuet-Higgins and E. Cokelet. The deformation of steep surface waves on water, I. A numerical method of computation. *Proceedings of the Royal Society A*, 350 :1–26, 1976.

[31] S. B. Nimmala, S. C. Yim, and S. T. Grilli. An efficient parallelized 3-D FNPF numerical wave tank for large-scale wave basin experiment simulation. *Journal of Offshore Mechanics and Arctic Engineering*, 135 :021104, 2013.

[32] W. T. Rankin. *Efficient parallel implementations of multipole based N-body algorithms.* PhD thesis, Duke University, Department of Electrical Engineering, 1999.

[33] Y.-L. Shao and O. M. Faltinsen. A harmonic polynomial cell (HPC) method for 3D Laplace equation with application in marine hydrodynamics. *Journal of Computational Physics*, 274 :312–332, 2014.

[34] H. G. Sung and S. T. Grilli. A note on accuracy and convergence of a third-order boundary element method for three dimensional nonlinear free surface flows. *Journal of Ships and Ocean Engineering*, 40 :31–41, 2005.

[35] H. G. Sung and S. T. Grilli. Numerical modeling of nonlinear surface waves caused by surface effect ships dynamics and kinematics. In *Proceedings of the 15th International Offshore and Polar Engineering Conference*, 2005.

[36] H. G. Sung and S. T. Grilli. Bem computations of 3d fully nonlinear free surface flows caused by advancing surface disturbances. *International Journal of Offshore and Polar Engineering*, 18(4) :292–301, 2008.

[37] K. Tanizawa. The state of the art on numerical wave tank. In *Proceedings of 4th Osaka Colloquium on Seakeeping Performance of Ships*, pages 95–114, 2000.

[38] R. Yokota. An FMM based on dual tree traversal for many-core architectures. *Journal of Algorithms and Computational Technology*, 7 :301–324, 2013.

[39] R. Yokota, J. P. Bardhan, M. G. Knepley, L. A. Barba, and T. Hamada. Biomolecular electrostatics using a fast multipole BEM on up to 512 GPUs and a billion unknowns. *Computer Physics Communications*, 182 :1272–1283, 2011.